Biogeochemistry (2021) 154:471–488
https://doi.org/10.1007/s10533-021-00797-5

Drivers of greenhouse gas emissions from standing dead trees in ghost forests

Melinda Martinez · Marcelo Ardón

Received: 24 September 2020 / Accepted: 16 April 2021 / Published online: 10 May 2021

Abstract Coastal freshwater forested wetlands are rapidly transitioning from forest to marsh, leaving behind many standing dead trees (snags) in areas often called 'ghost forests'. Snags can act as conduits for soil produced greenhouse gases (GHG) and can also be sources as they decompose. Thus, snags have the potential to contribute GHGs to the atmosphere, but emissions are not well understood. We assessed GHG emissions (carbon dioxide—CO_2, methane—CH_4, and nitrous oxide—N_2O) from snags and soils in five ghost forests along a salinity gradient on the coast of North Carolina, USA. Mean (± SE) soil GHG fluxes (416 ± 44 mg CO_2 m^{-2} h^{-1}, 5.9 ± 1.9 mg CH_4 m^{-2} h^{-1}, and 0.1 ± 0.06 mg N_2O m^{-2} h^{-1}) were ~ 4 times greater than mean snag GHGs (116 ± 15 mg CO_2 m^{-2} h^{-1}, 0.3 ± 0.09 mg CH_4 m^{-2} h^{-1}, and 0.04 ± 0.009 mg N_2O m^{-2} h^{-1}). Hydrological conditions and salinity influenced soil GHG fluxes between the two field campaigns, but snags were less predictable and more variable. Snag and soil CO_2/N_2O fluxes were influenced by similar environmental parameters. The drivers for soil and snag CH_4 however, were often not the same and at times oppositely correlated. Our results illustrate the need to further research into the drivers and importance of GHG emissions from snags, and the need to include tree stems into ecosystem GHG research.

Keywords Carbon dioxide (CO_2) · Methane (CH_4) · Nitrous oxide (N_2O) · Freshwater · Wetlands · Ghost forests

Responsible Editor: Jan Mulder

Supplementary Information The online version contains supplementary material available at https://doi.org/10.1007/s10533-021-00797-5.

M. Martinez (✉) · M. Ardón
Department of Forestry and Environmental Resources, North Carolina State University, Raleigh, NC 27695, USA
e-mail: mmarti13@ncsu.edu

M. Ardón
e-mail: mlardons@ncsu.edu

Introduction

Coastal freshwater forested wetlands contribute significantly to the global carbon (C) cycle through C sequestration and long-term storage (Kirwan and Megonigal 2013), but sea-level rise and climate change are driving transitions from forest to marsh (Krauss et al. 2018). Freshwater forested wetlands are affected by changes in storm frequency and sea level rise, leading to the creation of ghost forests, areas where trees are replaced by marsh vegetation (Kirwan and Gedan 2019). Ghost forests are expected to expand as the climate changes, which could have important implications for local and regional

greenhouse gas (GHG) budgets (carbon dioxide—CO_2, methane—CH_4, and nitrous oxide—N_2O), by altering emissions of GHGs from soils and standing dead trees (snags). It is unclear how the increase in ghost forests could affect the emission of GHGs from coastal landscapes.

Recent studies have focused on GHG emissions from trees (live and dead), revealing their importance to the global GHG budget (Covey and Megonigal 2019). It is estimated that vegetation may represent up to 22% of annual global CH_4 flux, contributing as much as 32–143 Tg CH_4 $year^{-1}$ (Carmichael et al. 2014). Standing dead mangrove trees have shown to exhibit higher CH_4 emissions than live mangrove trees (Jeffrey et al. 2019). Studies in tropical floodplains in the Amazon showed higher CH_4 emissions from live trees than peat soil surfaces nearby (Pangala et al. 2013). However, fewer studies have focused on snags, such as those found in ghost forests, which have the potential to transport soil produced gases as conduits, or produce them internally as wood decomposes (Carmichael et al. 2017; Jeffrey et al. 2019).

Production and emissions of GHGs from trees and soils in wetlands can be complex due to plant, microbial, and abiotic processes which can increase or decrease emissions to/from the atmosphere (Prendergast-Miller et al. 2011; Carmichael et al. 2014; Minick et al. 2019). Soil GHGs are affected by organic matter substrate availability, nutrient concentrations, soil redox conditions, pH, temperature, and salinity (Reddy and DeLaune 2008). Both CO_2 and CH_4 production in soils (and potentially snags) can be strongly affected by salinity, because sulfate (SO_4^{2-}) in seawater is a more energetically favorable electron acceptor, favoring microbial sulfate reduction over methanogenesis (Poffenbarger et al. 2011). The changes in availability of SO_4^{2-} can increase CO_2 production (Weston et al. 2011) and decrease CH_4 production (Neubauer 2013). Processes driving soil GHG emissions can be further complicated in snags because decomposition of wood releases labile carbon for methanogens and nitrate for denitrification, potentially increasing production of CH_4 and N_2O (Welch et al. 2019).

We assessed GHG emissions (CO_2, CH_4, and N_2O) from snags and soils in five ghost forests experiencing saltwater intrusion, flooding, and high rates of sea level rise (0.45 cm y^{-1}, Kopp et al. 2015) on the coast of North Carolina, USA. We conducted field campaigns over two summers to answer the following questions: (1) what is the composition and magnitude of GHG emissions from snags and do they differ from nearby soils? (2) do snag and soil GHG fluxes vary by site? (3) what influences snag GHG fluxes? (4) which GHGs contribute more to the radiative balance from soils and snags? We predicted that GHG emissions would be higher in soils than snags, and expected that emissions would differ among sites due to differences in salinity and hydrology. We explored various environmental factors that are known to affect GHG production.

Methods

Study sites

We examined five freshwater forested wetlands undergoing transition to marsh on the Albemarle Pamlico Peninsula (APP), North Carolina, USA (Fig. 1). The APP is a low-lying landform with the elevation of the majority of the peninsula within 1 m of mean sea level (Moorhead and Brinson 1995). The low elevation makes it more vulnerable to chronic disturbances from sea level rise, and saltwater intrusion (Moorhead and Brinson 1995; Poulter et al. 2006). Ghost forests in the APP have not been well classified, but a study by Ury et al. (2021 *In press*) estimated that ghost forests within the Alligator National Wildlife Refuge (total area: ~ 80,000 ha) take up approximately 3170 ha (~ 4% of total area) and have been increasing since 2012 (Smart et al. 2020). Wetlands within the APP generally experience low salinity (2–11 mS/cm), but can be subject to acute and chronic saltwater intrusion from hurricane storm surge or lack of freshwater from rivers and drought (Ardón et al. 2013; Manda et al. 2014).

Soil and snag GHG fluxes were measured along a salinity gradient with freshwater wetlands located along the northern portion of the APP, and brackish marshes found on the southern portion (Fig. 1). The five wetlands we selected are currently managed by either the state or US Fish and Wildlife Service and are experiencing various levels of forested wetland retreat: Palmetto-Peartree Preserve (PPP—Fig. 1-1), Pocosin Lakes National Wildlife Refuge (PC—Fig. 1-2), Swanquarter National Wildlife Refuge (SQ—Fig. 1-3), Gull Rock State Game Lands (GR—

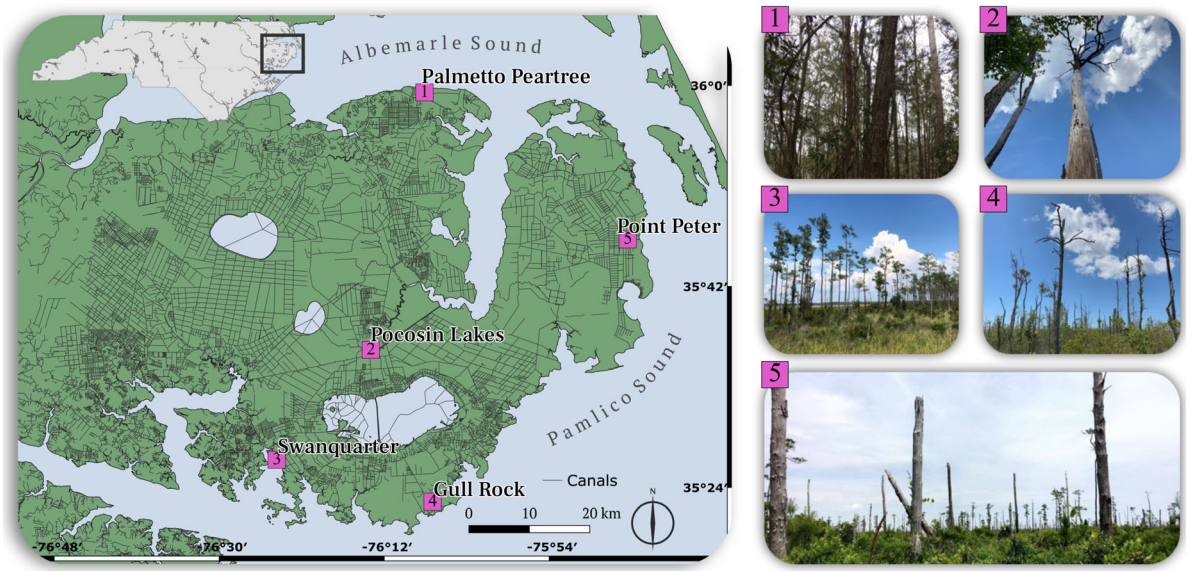

Fig. 1 Location of study in North Carolina, USA. Photos (right) shown of study areas with corresponding numbers on map (left). 1-1 Palmetto Peartree Preserve (PPP); 1-2 Pocosin Lakes National Wildlife Refuge (PC); 1-3 Swanquarter National Wildlife Refuge (SQ); 1-4 Gull Rock Game Lands (GR); 1-5 Point Peter Rd located within Alligator River National Wildlife Refuge (PP)

Fig. 1-4), and Point Peter Rd within the Alligator River National Wildlife Refuge (PP—Fig. 1-5). Palmetto Peartree Preserve is located near the Albemarle Sound, which is less saline than the pamlico sound (Corbett et al. 2007). The salinity gradient from the largely freshwater Albemarle Sound (less than 6 ppt) to the more brackish pamlico sound (> 12 ppt) is due to the number of inlets connecting the sounds to the ocean (Riggs et al. 1995). The vegetation from Gull Rock, Swanquarter, and Palmetto Peartree Preserve were further described by Taillie et al. (2019). The snags selected for all sites, were dead pine that had already lost most of the bark and few branches remaining (Fig. 1), except Pocosin Lakes which included cypress in addition to pine.

The two field campaigns were during the growing season, the first from May to October, 2018, and the second from May to August, 2019. The mean tree diameter at breast height (DBH) was 27 cm ± 1.17 (± SE) and 28.4 cm ± 1.33 for trees sampled in 2018 and 2019, respectively. During the first field campaign, measurements included weather parameters, soil temperature and conductivity, and GHG fluxes from snag stems and soils (Table 1). During the second field campaign, measurements were similar to 2018 with additional sampling described below (Table 1).

Greenhouse gas analysis

During the 2018 field campaign, we selected 5–10 snags at each site that were deemed stable (e.g. intact and not at risk of being felled), representative of the area, and were within 10 m of each other (n = 39). For the 2019 field campaign, we selected the same 5 snags from the previous year if possible except in Gull Rock, which had 5 additional snags selected as part of another study (n = 30) (Carmichael et al. 2021 *In Prep*). We were unable to resample all the same trees from 2018 during 2019 because a few (n = 8) had fallen during the two hurricanes in 2018 (Florence—September 14, 2018 and Michael—October 11–12, 2018). Snag and soil GHG fluxes were measured via a closed dynamic chamber technique using a portable gas analyzer (Gasmet DX4040, Vantaa, Finland) recording gas concentrations every 20 s for 10–20 min (10 min for snags, and 20 min for soils due to the larger chamber volume). The Gasmet library contained generic references of alpha- and beta-pinene, which are terpenes released by pine trees and have shown to interfere with CH_4 concentrations using laser-based analyzers and can exerted a strong bias on FTIR-based instruments (Kohl et al. 2019). The spectra for 2,3-dimethylbutane was also included

Table 1 List of parameters measured during both 2018 and 2019 field seasons

	Parameters measured	2018	2019
Snag GHG fluxes	CO_2, CH_4, and N_2O	X	X
Soil GHG fluxes	CO_2, CH_4, and N_2O	X	X
Weather	Temperature, rel. humidity, barometric, wind speed	X	X
Soils	Temperature and sp. conductivity	X	X
Soil characteristics	Organic matter, bulk density		X
Soil water extracted solutes	pH, NH_4-N, NO_3-N, PO_4-P, SO_4^{2-}, Cl^-		X
Ground water	Water level, water level deviation, sp. conductivity		X
Porewater	CO_2, CH_4, N_2O, SO_4^{2-}, Cl^-, NH_4-N, NO_3-N, PO_4-P		X

(only as an analytical help), however this component is not very likely to be present. From the snag chamber outlet, a 1 m gas tubing was connected to a drying agent (Drierite), and connected to Gasmet, then returned to tree chamber through a 1 m gas tubing connected to an additional outlet. The Gasmet flow rate was $\sim$ 1.5 L min^{-1} with a cell sample size of 0.4 L. The Gasmet uses Fourier transformation infrared spectroscopy, and has a detection range of up to 30,000 ppm—CO_2, 100 ppm—CH_4, and 5 ppm—N_2O. We used the closed static chamber technique with syringes when the Gasmet experienced battery or technical failures, sampling every 5 min over 40 min period (ESM 1). Approximately 15 mL of gas samples were stored in 12 mL pre-evacuated Exetainer vials (Labco–Lampeter, Wales, UK). Gases (CO_2, CH_4, and N_2O) were analyzed using an Agilent gas analyzer (7890A GC system—Santa Clara, CA) equipped with a methanizer and two detectors, flame ionization detector (FID) and micro-electron capture detector (ECD), for CH_4 and N_2O analysis respectively. The ranges for the GC were up to 10,000 ppm—CO_2, 100 ppm—CH_4, and 5 ppm—N_2O.

Snag chambers were temporarily attached during measurements at various heights depending on optimal sealing conditions but were generally near $\sim$ 60–70 cm from soil surface. Snag chambers were made of clear, flexible polycarbonate sheets (0.76 mm thick) modeled after Siegenthaler et al. (2016) and varied in size (Chamber 1: 45 × 25 × 2.5 cm & Chamber 2: 29 × 20.5 × 2.5 cm, length × width × depth respectively) based on snag diameters (ESM 1). Soil chambers (30 cm diameter) were modeled after Winton and Richardson (2016) and placed 10 cm into the ground within 1–2 m from selected trees (n = 31 in 2018; n = 30 in 2019). GHG flux measurements were repeated every other month over the growing season for each field campaign (n = 2 per site per year). Both soil and snag chambers had temperature data loggers during gas sampling, measuring every minute inside the chamber using iButtons, which have an accuracy of ± 0.5 °C (Maxim Integrated, San Jose, CA). Fluxes, expressed as mg m^{-2} h^{-1}, were determined using a linear and non-linear modelling approach called HMR after Hutchinson and Mosier (1981) and described in detail by Pedersen et al. (2010). The R package '*HMR*' was used to calculate regressions and kept only significant ($p < 0.1$) correlations (Pedersen et al. 2010). Snag stem GHG fluxes were calculated by estimating the stem surface area up to the chamber measurement, assuming cylindrical stem, and is expressed as mg $stem^{-1}$ h^{-1}. CH_4 and N_2O fluxes were also converted to CO_2 equivalents on a 100 year time horizon by multiplying by 45 and 270, respectively (Neubauer and Megonigal 2015).

In order to scale up GHG fluxes, snag and live tree density estimates were recorded within a 100 m^2 plot for each site (Table 2). Within the plot, snag and live tree DBH was measured for trees greater than 3 cm DBH. Basal area was calculated using the equation: $\pi \times (DBH/2)^2$, with DBH converted to meters. Soil surface area was estimated by subtracting basal area of live trees and snags (Pangala et al. 2017). Scrubs/shrubs basal area were not measured. Snag GHG $CO_{2(eq)}$ equivalent fluxes were upscaled by calculating the surface area up to 1.4 m, assuming the stem was cylindrical, multiplied the median GHG flux rate by

Table 2 Site characteristics from two 100 m^2 plots per site, including mean (± SE) tree density

Site	Dominant vegetation	Understory vegetation	Dead tree density (tree m^{-2})	Live tree density (tree m^{-2})
PPP 35° 59.502′N 76° 8.569′W	*Pinus taeda*	*Morella cerifera.* Pine saplings	0.08 ± NA	0.14 ± NA
PC 35° 35.974′N 76° 13.966′W	*Taxodium distichum, Nyssa aquatic, Pinus* spp.	*Morella cerifera; Nyssa sylvatica, Cladium jamaicense, Typha latifolia*	0.09 ± 0.007	0.03 ± 0.01
PP 35° 46.251′N 75° 45.406′W	*Pinus serotine*	*Morella cerifera,* pine saplings	0.06 ± 0.04	0.04 ± 0.02
GR 35° 21.884′N 76° 6.912′W	*Pinus* spp, *Acer rubrum*	*Iva frutescens, Typha latifolia,* pine saplings	0.08 ± 0.02	0.045 ± 0.02
SQ 35° 26.224′N 76° 23.763′W	*Pinus* spp	*Iva frutescens, Cladium jamaicense, Juncus roemerianus*	0.06 ± 0.01	0.025 ± 0.007

site, and then summed the snag stem GHGs within the 100 m^2 plot.

Weather parameters

To examine environmental drivers of GHG fluxes, environmental parameters such as air temperature, relative humidity, and barometric pressure were measured continuously every minute during sampling events using a Kestrel monitoring device (Kestrel 5000 Environmental Meter, Minneapolis, MN).

Water chemistry

Slotted PVC wells (5.08 cm diameter and inserted 1 m into ground) were installed on February 2019 at each site to estimate water levels and conductivity of soil solution (HOBO Onset Water Level: U20L-04, Conductivity: U24-00; Solinst Level Logger: Model 3001). Loggers recorded water level and conductivity every 15 min throughout the growing season (Fig. 2). Precipitation has been shown to influence water table depth leading to quick increases above ground level (Minick et al. 2019), therefore daily precipitation and temperature data were extracted from Climate Engine (METDATA/gridMET) for each site (Huntington et al. 2017).

To measure soil solutes and porewater GHGs, porewater sippers were also installed in February 2019 at each site near three selected snags at two depths 15 cm (n = 15) and 30 cm (n = 15) (ESM 1). Porewater sippers were constructed from plastic tubing attached to an air stone (4 cm long × 2 cm diameter). The air stone was housed inside a 2.54 cm diameter PVC, which was slotted near measuring depth and wrapped in a filter sock to prevent silt and sediment

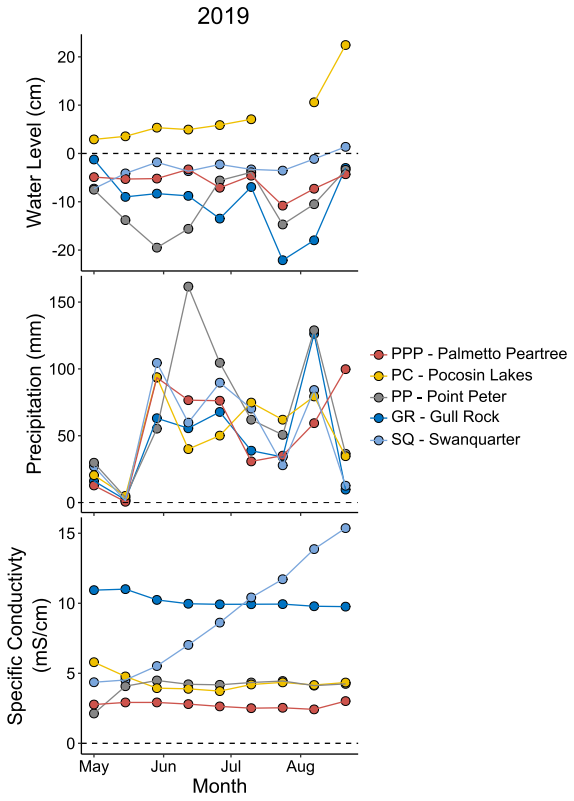

Fig. 2 Median biweekly water dynamics for each site during the 2019 growing season. Precipitation is cumulative for each 2-week interval. Water level data at PC was not logged from Jun 15 to Aug 1 due to logger malfunction

build up (Wilson et al. 2018). A 60-mL syringe was used to create a vacuum to extract soil solution. Porewater was drawn after soil GHG sampling and measured for GHG concentrations, NO_3-N, NH_4-N, Cl^-, PO_4-P, and SO_4^{2-}. To measure GHG concentrations, approximately 6–7 mL of soil solution was inserted into a 12 mL pre-evacuated Exetainer vial and was later filled with ultra-pure nitrogen gas. GHG concentrations were measured using headspace equilibrations techniques after adjusting to room temperature (Helton et al. 2014).

To measure porewater solutes, an additional 30–40 mL of soil solution was extracted from the sippers and filtered through 0.7 µm GFF filter for porewater solutes and stored in scintillation vials. Exetainer samples were stored upside down and kept cool until analysis, and scintillation vials were kept cool during transport and frozen until analysis. NH_4-N and PO_4-P were measured on a Seal Analytical AA3 Segmented Flow Analyzer, while SO_4^{2-}, Cl^-, and NO_3-N were analyzed on a Metrohm 930 Flex Ion Chromatograph using chemical suppression and conductivity detection. The measured values on both analyzers were calibrated using standards and were within 10% of expected values.

Soil geochemistry

For each site, four sets of soil half-cores were collected on June 2019 using a Russian Peat corer (5 cm diameter 50 cm length; AMS Inc. American Falls, ID). Cores were sectioned in the field into increments of 5 cm and placed in airtight sampling bags (Whirl–Pak, Madison, WI), and kept cool until lab analysis. One core was used for bulk density and organic matter measurements, the other three were used for water extractable solutes after sieving through a 2 mm sieve. Water extractable solutes (NO_3-N, NH_4-N, Cl^-, PO_4-P, and SO_4^{2-}) and pH were determined for each depth following methods from Helton et al. (2019). The soil subsample for bulk density was weighed and dried at 60°C, and re-weighed to determine soil water content, and bulk density. The dry soil was then placed in muffle furnace at 550 °C for 4 h to measure soil organic matter by loss on ignition (LOI). Soil volumetric water content was calculated by using the following equation: $\frac{wet\ mass - dry\ mass(g)}{dry\ mass(g)} \times \frac{bulk\ density\left(g\ cm^{-3}\right)}{density\ of\ water\ (g\ cm^{-3})}$.

Statistics

Due to the lack of normality in the data, we used an aligned rank transformation non-parametric factorial analysis to test for significant differences in GHG fluxes between years, sites, and their interaction effect for both snag and soil fluxes (Wobbrock et al. 2011). Kruskal–Wallis was used to test significant differences in porewater chemistry across sites and between $CO_{2(eq)}$ equivalent gases. Dunn's multiple pairwise comparisons were then used for post-hoc analysis when Kruskal–Wallis showed significant differences, with a Bonferroni p-value adjustment ($p < 0.05$). A one-way ANOVA was used to test significant differences in soil water extractable solutes (NH_4-N, PO_4-P, Cl^-, NO_3-N, and SO_4^{2-}), and soil properties (pH, dry bulk density, organic matter, %C, and %N) across sites after log transformations showed normality. Soil extractable solutes and properties were averaged from

the top 15 cm (5, 10, and 15 cm) depths for each soil core (n = 3 per site). Tukey HSD was then used for post-hoc analysis when ANOVA was significant ($p < 0.05$), although we also considered marginally significant differences ($p < 0.1$). Spearman rank correlations were used to explore relationships between snag and soil GHG fluxes, and potential environmental drivers (weather, soil GHG fluxes, porewater GHG concentrations, porewater solutes, and water parameters). Porewater nutrient data was averaged by site and month combining 15 cm and 30 cm soil solution. All analyses were conducted in R (version R 3.6.1) using *stats* and *PMCMR* packages (Pohlert 2014; R Core Team 2020).

Results

Site characteristics

During the first field campaign in 2018, our sites received on average 1.5 times the rainfall (896 mm) compared to the 2019 sampling campaign (666 mm, which is similar to the long-term median ± SE of 672 mm ± 22, ESM 2). Mean temperature (± SE) during 2018 field campaign was 26.4 ± 0.2 °C, and 25.4 ± 0.24 °C during 2019 field campaign. Water level referenced to the ground varied from approximately − 13 cm at Gull Rock and Point Peter, to 4.7 cm Pocosin Lakes in 2019 (Fig. 2). Mean specific conductivity from groundwater wells ranged from ∼ 3 mS cm in Palmetto Peartree and Point Peter, to ∼ 10 mS/cm in Swanquarter and Gull Rock. Specific conductivity remained relatively constant within each site, except Swanquarter which increased from 4.56 to 14.3 mS/cm throughout the growing season (Fig. 2).

Mean soil extractable solutes differed across sites for all solutes and pH, except for NO_3-N, which was low across all sites (Table 3). Soil Cl^- and SO_4^{2-} concentrations were 15–26 times higher in Swanquarter than concentrations in Point Peter (Table 3). Soil pH was also significantly higher in Swanquarter (1.5 greater) than all other sites (Table 3). Soil NH_4-N showed a similar trend, with lower concentrations in Point Peter and Palmetto Peartree (∼ 0.08 mg/L), and the highest in Swanquarter (0.71 mg/L, Table 3). Soil PO_4-P was lower in Gull Rock, Point Peter, and Palmetto Peartree (∼ 25 µg/L), compared to Swanquarter and Pocosin Lakes (∼ 70 µg/L, Table 3). Soil bulk density was highest in Palmetto Peartree Preserve (1.05 g/cm^3), and lowest in Swanquarter (0.15 g/cm^3). Soil organic matter and %C was lowest in Palmetto Peartree Preserve (∼ 7%) compared to all other sites (Table 4).

Porewater dynamics

Porewater chemistry and GHG concentrations varied across all sites (Fig. 3). Porewater CO_2 concentrations ranged from 2.64 to 90.57 mM (Fig. 3). Point Peter had the lowest concentration of porewater CO_2 (12.39 mM), while Palmetto Peartree and Swanquarter had the highest (44 and 32 mM respectively) and most variable concentrations (Fig. 3a). Porewater CH_4 concentrations ranged from 0.06 to 566 µM and were different among sites (Fig. 3b). Porewater N_2O concentrations ranged from 0 to 2.36 µM but were not significantly different among sites (Fig. 3c).

Table 3 Mean soil extractable solutes for each site from 0 to 15 cm depth range

Site	pH	NH_4-N (mg/L)	PO_4-P (µg/L)	Cl^- (mg/L)	NO_3-N (mg/L)	SO_4^{2-}(mg/L)
PPP	5.90 ± 0.23^a	0.08 ± 0.01^b	22.03 ± 3.70^a	42.16 ± 8.83^c	0.06 ± 0.01	2.79 ± 0.54^c
PC	5.94 ± 0.14^a	0.19 ± 0.03^a	89.60 ± 18.58^b	64.13 ± 4.56^b	0.07 ± 0.01	6.45 ± 0.40^a
PP	4.71 ± 0.05^b	0.09 ± 0.01^b	35.72 ± 11.60^{ac}	32.38 ± 2.83^c	0.09 ± 0.02	0.97 ± 0.09^b
GR	5.57 ± 0.07^a	0.33 ± 0.03^a	24.05 ± 6.63^a	186.09 ± 6.17^a	0.08 ± 0.01	11.47 ± 2.77^a
SQ	7.30 ± 0.08^c	0.71 ± 0.03^c	65.23^a ± 10.47^{bc}	491.54 ± 4.29^d	0.06 ± 0.02	26.25 ± 1.37^d

Means (± SE) were compared among sites

Different letters indicate significant differences ($p < 0.05$)

Table 4 Mean soil (0–15 cm depth) characteristics for each site

Site	Soil water content	Dry bulk density (g/cm^3)	Organic matter (%)	Soil C (%)	Soil N (%)
PPP	0.56 ± 0.08^{b}	1.05 ± 0.29^{b}	9.36 ± 5.10^{b}	6.33 ± 1.04^{c}	0.33 ± 0.05^{b}
PC	1.3 ± 0.15^{a}	0.40 ± 0.13^{ab}	64.93 ± 12.27^{a}	24.23 ± 3.82^{a}	1.28 ± 0.20^{a}
PP	0.96 ± 0.26^{a}	0.19 ± 0.05^{a}	88.32 ± 0.87^{a}	58.21 ± 0.83^{b}	1.09 ± 0.02^{a}
GR	0.97 ± 0.09^{a}	0.25 ± 0.05^{a}	71.24 ± 9.79^{a}	35.55 ± 3.23^{a}	1.30 ± 0.14^{a}
SQ	0.98 ± 0.06^{a}	0.15 ± 0.02^{a}	64.95 ± 5.33^{a}	24.38 ± 4.08^{a}	1.46 ± 0.23^{a}

Mean (± SE) were compared among sites

Different letters indicated significant differences ($p < 0.05$)

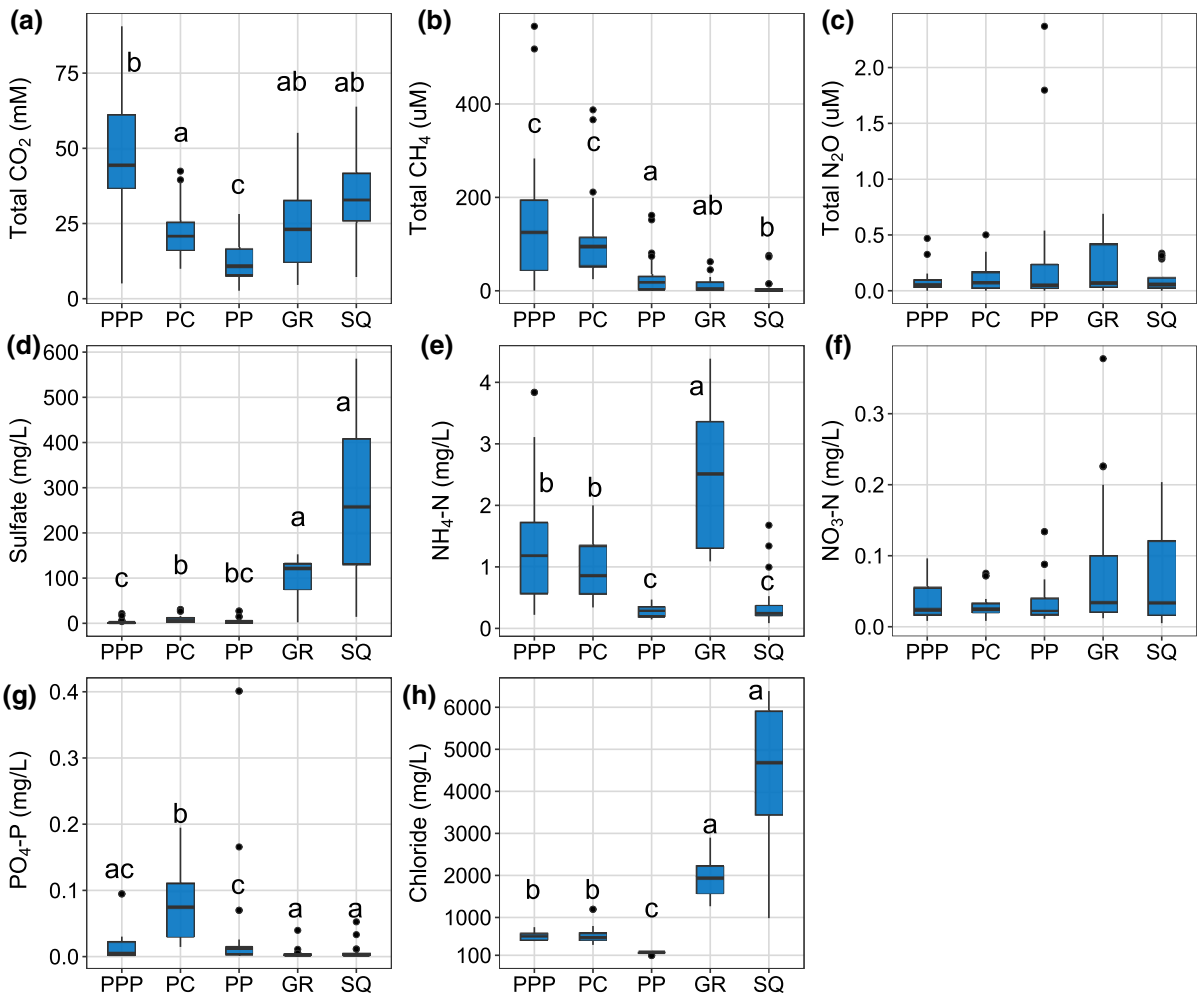

Fig. 3 Porewater chemistry and greenhouse gas concentrations for each site from 2019 only (15 and 30 cm combined). Solid line represents median, whiskers represent 5th and 95th percentiles, and dots are outliers. Different letters show significant differences between sites ($p < 0.05$)

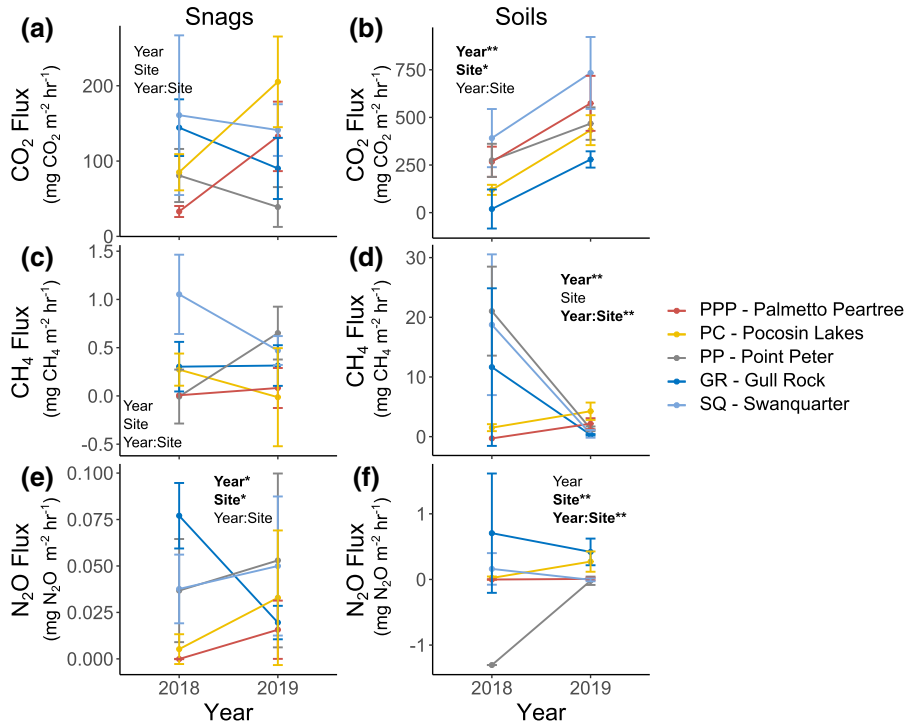

Fig. 4 Mean (± SE) GHG fluxes for tree and soil chambers by year and site. Significant factors are in bold; (**) indicates $p < 0.05$ and (*) indicates $p < 0.1$. Note different scales between respective tree and soil GHG fluxes

Porewater NH_4-N ranged from 0.2 to 4.3 mg/L across all sites. Swanquarter and Point Peter had significantly lower NH_4-N (0.2–0.4 mg/L), and Gull Rock (2.5 mg/L) had the highest (Fig. 3e). Porewater NO_3-N was low (< 0.09 mg/L) in all sites (Fig. 3f). PO_4-P concentrations were significantly lower in Swanquarter and Gull Rock (0.004–0.006 mg/L) compared to Pocosin Lakes having the highest concentrations (0.07 mg/L). Porewater SO_4^{2-} was also significantly different among sites, with higher concentrations in Swanquarter and Gull Rock (99–266 mg/L), compared to Pocosin Lakes (9.5 mg/L), Point Peter (5.3 mg/L), and Palmetto Peartree (3.6 mg/L). Similar to sulfate, chloride concentrations were also significantly higher in Gull Rock and Swanquarter (1969 and 4943 mg/L respectively), and much lower in Point Peter, (163 mg/L; Fig. 3h).

GHG fluxes

Overall GHG fluxes were ~ 4 times higher in soils (mean ± SE GHG fluxes: 416 ± 44 mg CO_2 m^{-2} h^{-1}, 5.9 ± 1.9 mg CH_4 m^{-2} h^{-1}, and 0.1 ± 0.06 mg N_2O m^{-2} h^{-1}) than snags (mean ± SE GHG fluxes: 116 ± 15 mg CO_2 m^{-2} h^{-1}, 0.3 ± 0.09 mg CH_4 m^{-2} h^{-1}, and 0.04 ± 0.009 mg N_2O m^{-2} h^{-1}) for both years. When scaling snag fluxes per stem surface (mean stem GHG fluxes: 97 ± 12 mg CO_2 $stem^{-1}$ h^{-1}, 0.21 ± 0.08 mg CH_4 $stem^{-1}$ h^{-1}, 0.02 ± 0.005 mg N_2O $stem^{-1}$ h^{-1}), soils were ~ 5 times higher. Both soils and snags were sources and sinks of all GHGs. There were a total of 68 and 81 tree chamber measurements, and 36 and 77 soil chamber measurements in 2018 and 2019, respectively. The number of measurements that met our flux validity criteria for both years combined varied for each GHG with CO_2 having higher percentages for both snag (88%) and soil (88%) measurements, followed by CH_4 (55%—snag, 69%—soil), and N_2O (55%—snag, 67%—soil). Snag CO_2 fluxes ranged from − 297 to 1107 mg CO_2 m^{-2} h^{-1} (n = 131), while soil CO_2 fluxes ranged from − 369 to 2347 mg CO_2 m^{-2} h^{-1} (n = 100). Snag CH_4 emissions ranged from − 3.2 to 3.1 mg CH_4 m^{-2} h^{-1} (n = 83), while soil CH_4 emissions ranged from − 20 to 114 mg CH_4 m^{-2} h^{-1} (n = 78). Snag N_2O fluxes ranged from − 0.13 to 0.45 mg N_2O m^{-2} h^{-1} (n = 83), and soil N_2O fluxes ranging from − 1.3 to 2.5 mg N_2O m^{-2} h^{-1} (n = 76). When considering the snag density

Table 5 Median (± SE) snag stem GHG fluxes per site

Year	Site	Snag stem GHG fluxes		
		mg CO_2 $stem^{-1}$ h^{-1}	mg CH_4 $stem^{-1}$ h^{-1}	mg N_2O $stem^{-1}$ h^{-1}
2018	PPP	13.7 ± 8.6	0 ± NA	0 ± NA
2018	PC	96.7 ± 22.4	0.3 ± 0.2	0.01 ± 0.01
2018	PP	39.8 ± 19	− 0.09 ± 0.2	0.02 ± 0.02
2018	GR	90.5 ± 24.2	0.2 ± 0.2	0.05 ± 0.01
2018	SQ	114 ± 67.9	0.8 ± 0.3	0.03 ± 0.01
2019	PPP	130.4 ± 57.6	− 0.08 ± 0.2	0.02 ± 0.02
2019	PC	229.6 ± 48.1	0.3 ± 0.8	0.02 ± 0.02
2019	PP	22.5 ± 17.9	0.4 ± 0.1	0.02 ± 0.02
2019	GR	85 ± 43	0.3 ± 0.2	0.02 ± 0.01
2019	SQ	99.2 ± 22.8	0.3 ± 0.1	0.02 ± 0.02

Cylindrical surface area of stem was calculated using measured DBH up to chamber measurement height (varied per snag)

and upscaling $CO_{2(eq)}$ GHGs for snag stems and soil area (without tree basal area) within a 100 m^2 plot at each site, we estimated snag GHGs contribute an additional 200–1200 mg $CO_{2(eq)}$ hr^{-1} (Table 6). The scaling of GHGs are conservative estimates due to lack of precise soil surface area.

Snag CO_2 fluxes were not significantly different between years (2018—wet & 2019—dry) nor among sites and did not have an interaction effect (Fig. 4a). Snag CO_2 increased 3 and 10 times for Pocosin Lakes and Palmetto Peartree, respectively, while Point Peter and Swanquarter remained similar across years (Table 5). Soil CO_2 fluxes were different between years ($p = 0.0005$), and among sites ($p = 0.05$, Fig. 4b). Soil CO_2 fluxes were approximately 2 times higher in 2019 (502 mg CO_2 m^{-2} h^{-1}) than in 2018 (240 mg CO_2 m^{-2} h^{-1}) and were 2 times higher in Palmetto Peartree (532 mg CO_2 m^{-2} h^{-1}) than Gull Rock (232 mg CO_2 m^{-2} h^{-1}). There were no significant differences in snag CH_4 fluxes among sites, between years, or their interaction effect (Fig. 4c). Snag CH_4 fluxes in Gull Rock (0.30 mg CH_4 m^{-2} h) were higher than Palmetto Peartree (0.07 mg CH_4 m^{-2} h^{-1}), while all other sites slightly increased from 2018 to 2019 (Fig. 4c). Snag stem CH_4 fluxes in Point Peter (2018) and Palmetto Peartree (2019) were sinks instead of sources unlike all other sites (Table 5). The interaction between year and sites was significant for soil CH_4 fluxes ($p = 0.0003$), although soil CH_4 fluxes differed between years ($p = 0.01$) but not among sites ($p = 0.19$, Fig. 4d). There was twice as much more variation in soil CH_4 fluxes in 2018 for Swanquarter, Gull Rock and Point Peter, compared to 2019, unlike Palmetto Peartree and Pocosin Lakes which had the least variation in 2018 and slightly increased from 2018 to 2019 (Fig. 4d). Snag stem N_2O fluxes were highly variable both years (Fig. 4e) and marginally significant among sites ($p = 0.07$), and between years ($p = 0.09$). Gull Rock was the only site that decreased in snag stem N_2O fluxes, while all other sites slightly increased from 2018 to 2019 (Table 5; Fig. 4e). Soil N_2O fluxes were not different between years, but were among sites ($p = 0.001$), and had interaction effects ($p = 0.006$, Fig. 2f). Soil N_2O fluxes were higher and more variable ($\sim$ 3 times more variable) in 2018 for Gull Rock and decreased in variability in 2019 (Fig. 4f). Pocosin Lakes was the only site that was converted from an N_2O sink in 2018 (-0.0012 mg N_2O m^{-2} h^{-1}) to a source in 2019 (0.008 mg N_2O m^{-2} h^{-1}), while Point Peter remained a N_2O sink both years but was reduced from − 1.3 to − 0.02 mg N_2O m^{-2} h^{-1} from 2018 to 2019 (Fig. 4f).

GHG correlations

Snag GHG fluxes did not correlate with their respective soil GHG flux measurements (data not shown). Snag CO_2 fluxes were correlated negatively with porewater N_2O ($\rho = -0.52$), and relative humidity ($\rho = -0.27$) and positively with temperature

(ρ = 0.44), porewater CO_2 (ρ = 0.39), and PO_4-P (ρ = 0.33, ESM 3). Snag CH_4 fluxes were positively correlated with precipitation (ρ = 0.59) and NO_3-N (ρ = 0.49), and negatively correlated with DBH (ρ = − 0.62) and porewater CH_4 (ρ = − 0.48). Snag N_2O fluxes were positively correlated with NO_3-N (ρ = 0.34), and negatively correlated with porewater CH_4 (ρ = − 0.42) and water level (ρ = − 0.38). Soil and snag CH_4 fluxes had some measured parameters that were oppositely correlated (ESM 3). Soil CO_2 fluxes were positively correlated with water level deviation (ρ = 0.54), Cl^- (ρ = 0.50), precipitation (ρ = 0.49), and SO_4^{2-} (ρ = 47), and negatively correlated with porewater N_2O (ρ = − 0.42) and porewater CH_4 (ρ = − 0.40, ESM3). Soil CH_4 fluxes were positively correlated with porewater CH_4 (ρ = 0.44), and negatively correlated with Cl^- (ρ = − 0.64) and NO_3-N (ρ = 0.57). Soil N_2O fluxes were positively correlated with NH_4-N (ρ = 0.7) and specific conductivity (ρ = 0.64), and negatively correlated with PO_4-P (ρ = − 0.29).

Radiative forcing

CO_2 fluxes remained the dominant radiative balance contributor for snag fluxes both years (10 and 120 times higher than CH_4 and N_2O respectively), but differed by year for soil fluxes. In 2018, soil $CH_4{\cdot}CO_{2(eq)}$ fluxes were within the same range as soil CO_2 fluxes, and $N_2O{\cdot}CO_{2(eq)}$ fluxes were significantly less (Fig. 5). Soil CO_2 fluxes in 2019 were the dominant contributor followed by CH_4, and much less for N_2O fluxes (Fig. 5).

Discussion

We found evidence to support our prediction regarding differences between snag and soil GHG fluxes. Our results showed that soil GHG fluxes were ∼ 4 times higher in soils than snag GHG fluxes for all sites and years (Fig. 2). Our second prediction was that snag and soil GHG fluxes would differ by site, which we found to be true only for snag N_2O fluxes, and all soil GHG fluxes (Fig. 4). We were surprised to see that snag GHG fluxes were not as significantly affected by differences in soil hydrologic conditions and salinity as soil GHG fluxes, and had much more variability both years (Fig. 4a, c, e). There were some differences in correlations between snag GHG fluxes and soil GHG fluxes when compared to environmental parameters. For example, soil CH_4 fluxes were strongly negatively correlated with porewater CO_2, Cl^- and SO_4^{2-}, while snag CH_4 fluxes were positively correlated with these same parameters (ESM 3). Environmental parameters that influence soil CH_4 production or inhibition, are not the same in snags and are often oppositely correlated. It is important to note however that our snag GHG flux estimates are conservative because they were not measured directly at the base of snags. Studies have shown that tree stem GHG flux rates have been known to decrease either linearly or

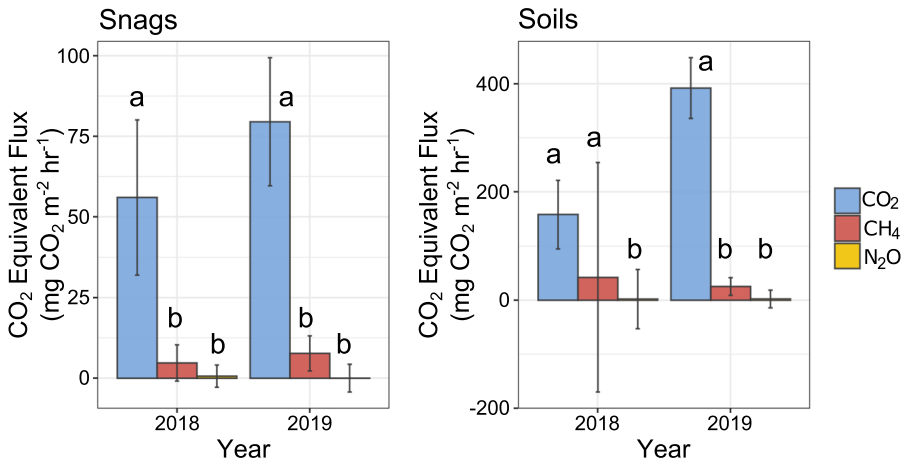

Fig. 5 Median (± SE) CO_2 equivalent flux (CO_2, CH_4 × 45, N_2O × 270) for soils and tree fluxes by year. Note different scales between soils and tree fluxes. Different letters indicate significant differences between CO_2 equivalent GHGs within respective year

exponentially with increasing stem height sampling position (Pangala et al. 2017; Jeffrey et al. 2019). Lastly, regarding our last prediction about the contribution of snag $CO_{2(eq)}$, we found that CH_4 and $N_2O{\cdot}CO_{2(eq)}$ from snags do not contribute the same amount as CO_2 (Fig. 3). As expected CO_2 gases were the largest contributor in soils during the dry year (2019), but during the wet year (2018) the CH_4 contribution could be just as high as CO_2 (Fig. 5). Overall, we found that flooding conditions and soil characteristics can substantially affect soil GHGs, but the magnitude and direction of snag GHGs can be less predictable.

GHG fluxes

Precipitation had an important effect on soil GHG fluxes. The cumulative precipitation in 2018 was the third wettest growing season since 1979 (Climate Engine gridMET; Huntington et al. 2017), while the drier 2019 growing season was near the overall median (ESM 2). Because the water table was much lower throughout most of the growing season in 2019 (Fig. 2), soil CO_2 fluxes increased at all sites (Fig. 4b), soil CH_4 fluxes were reduced in variability, with the exception of Palmetto Peartree (Fig. 4d), and soil N_2O fluxes decreased in three out of the five sites (Gull Rock, Point Peter, and Swanquarter) (Fig. 4). The increase in soil CO_2 fluxes could have been caused by increased carbon mineralization due to a lower water table, or due to higher plant root/microbial respiration. In a microcosm experiment using soils from a nearby site, CO_2 fluxes increased under intermittently flooded conditions, compared to flooded conditions (Helton et al. 2019). The decrease in water levels also caused a decrease in variability and increased the potential for CH_4 oxidation near soil surfaces for all sites except Palmetto Peartree and Pocosin Lakes. The decrease in soil N_2O fluxes in Gull Rock and Swanquarter could have been caused by an increase in completed nitrification (decrease in denitrification), or due to a decrease in soil N due to increased herbaceous vegetation uptake given the drier conditions in 2019 (Chapin and Matson 2011).

Although soil CH_4 fluxes decreased during the drier year (2019), snag CH_4 fluxes slightly increased for Point Peter, and Palmetto Peartree, slightly decreased for Swanquarter and Pocosin Lakes, and remained similar for Gull Rock (Fig. 4c). The increase in snag CH_4 fluxes during the drier year could be caused by stem release of CH_4 produced in deeper saturated soils diffusing up snag. The drop in water levels could have induced CH_4 release through the open internal cavities of the snags, allowing gas to transport in trees by molecular diffusion, and concentration gradients (Megonigal et al. 2020). Transport through the snag allows CH_4 to bypass the oxidation that occurs in upper horizons of soils, but it is also possible that CH_4 is oxidized as it is transported up the snag stem, which would explain the decrease in snag CH_4 fluxes in some sites (Hornibrook et al. 1997). The contrasting response of snags and soils CH_4 fluxes to changes in precipitation illustrate the complexity in drivers of soil–plant-atmosphere interactions, especially in snags which appear to be more variable than soils.

Snag N_2O fluxes also had significant increases from 2018 to 2019 (except at Gull Rock), which could have been related to the increases in soil N_2O fluxes, although the correlation between snag and soil N_2O fluxes was not significant. The difference between years highlights the importance of snag N_2O fluxes under different hydrologic conditions. Previous studies have suggested a decrease in live tree stem CH_4 and N_2O emissions and variability during drier conditions compared to wetter conditions (Barba et al. 2019b), but our study shows mixed responses, which demonstrates the complexities in GHG production from snags (Fig. 4a, c). During the wet year (2018), Point Peter was a major N_2O sink in soils which can occur in high water content and low inorganic N availability (Neubauer and Megonigal 2015). During drier years, such as 2019, snag N_2O gases need to be taken into account because of their high global warming potential.

Porewater dynamics

Porewater solutes showed distinct characteristics between sites (Fig. 3). Trees have been shown to act as conduits for the atmospheric flux of GHG from wetlands (although the source of origin may vary), therefore it is possible that the snags were emitting GHGs from deeper soils. The mechanisms of gas transport in snags, however, differs from live trees because there is no active water transport through the xylem and phloem (Megonigal et al. 2020). It is most likely that snag GHGs are mostly driven by molecular

diffusion driven by concentration gradients from soil and porewater.

Swanquarter had higher snag CH_4 fluxes during the wetter year (2018) and was reduced during the drier year (2019). Out of all sites, Gull Rock had among the highest porewater NH_4-N (Fig. 3) and the second to highest soil extractable NH_4-N after Swanquarter (Table 3). The high amount of NH_4-N in soil solution at Gull Rock and Swanquarter is most likely due to salinization causing displacement of NH_4^+ ions by marine cations (Ardón et al. 2013). Although Swanquarter was more saline and had higher concentrations of SO_4^{2-} (Table 3 & Fig. 4), Gull Rock was significantly higher in porewater NH_4-N, most likely due its proximity to a waterfowl impoundment (Winton and Richardson 2017). Herbivorous birds contribute to the amount of N via digestion and excretion of consumed plants making N more soluble and mobile (Winton et al. 2016). High amounts of NH_4-N can suppress CH_4 consumption by oxidizers, potentially increasing CH_4 concentrations, which could explain why snag CH_4 fluxes were high in Swanquarter and Gull Rock in 2018 (Morse et al. 2012; Ardón et al. 2018).

GHG correlations

The lack of correlation between snag and soil GHG fluxes suggests that snag GHG production is complex and may be indirectly affected by soil GHG production. The drivers that produce soil CH_4 and snag CH_4 fluxes were not the same, and at times oppositely correlated (ESM 3). It is possible that the GHGs from snags depend on production of gases in the soils and undergo various processes within the trunk including oxidation/consumption of CH_4 and N_2O, which has been shown in other studies (Machacova et al. 2016; Carmichael et al. 2017; Jeffrey et al. 2021). This hypothesis is even more likely considering the snag chambers were placed 60–70 cm from the ground, thus are conservative. This also helps explain the disconnect between environmental parameters that influence soil CH_4 versus snag CH_4 (ESM 3). Snag CH_4 and N_2O fluxes were negatively correlated with DBH, which was similar to a previous study (Pangala et al. 2017), although there may be different reasons. In the Amazonian study by Pangala et al (2017), young live tree stems emitted more CH_4 than mature live tree stems. In our study it is likely that smaller snag stems emit higher concentrations of CH_4 because there is less time for oxidation through the sapwood as opposed to larger diameter snags.

Some of the environmental parameters that influence soil CO_2 and N_2O fluxes were similar to those of snag CO_2 and N_2O fluxes. For example, CO_2 fluxes for soils and snags are both positively correlated with temperature, porewater CO_2, and water level deviation, and both are negatively correlated with relative humidity. This suggests that faster decomposition occurs during warmer and drier conditions in both snags and soils (ESM 3). The positive correlation between soil CO_2 and NO_3-N implies that available inorganic N may help produce CO_2 indirectly because of its role in the microbial community (Zhang et al. 2019). N_2O production in soils and snags were also both positively correlated with NO_3-N, SO_4^{2-}, and Cl^-, and both negatively correlated with PO_4-P. The inorganic N availability in soils and the periodic alterations in soil water content can trigger nitrification and denitrification processes and produce N_2O in soils (Moldaschl et al. 2021). Snag N_2O emissions could be formed within snag tissues, similarly to CH_4 emissions, by a different set of microorganisms that live in association with trees (Machacova et al. 2019). *Paxillus involutus (Batsch) Fr.* and *Tylospora fibrillosa (Burt.)* are two ectomycorrhizal fungi found to form symbiotic associations with pine tree roots in acidic temperate soils (Prendergast-Miller et al. 2011). They become highly competitive when inorganic N concentrations are high, thus producing N_2O through nitrate reduction under low O_2 conditions (Prendergast-Miller et al. 2011). The soils at Gull Rock were conducive to these types of symbiotic fungi due to acidity (pH $\sim$ 5) and high amounts of NH_4-N. This could explain why soil and snag N_2O fluxes were high at Gull Rock, and thus had higher snag N_2O fluxes than all other sites especially during the wet year, 2018 (Fig. 4e).

Radiative forcing

Soil CO_2 fluxes were the dominant radiative balance contributor for both years, although during the wet year (2018) CH_4 fluxes contributed as much to radiative forcing as CO_2 (Fig. 5). For snags, CO_2 fluxes were the dominant contributor, although its contribution was slightly higher in 2019 (drier year). Although snag CH_4 and N_2O fluxes did not contribute as much as CO_2 fluxes it is still important to take into

Table 6 Upscaled snag stem and soil $CO_{2(eq)}$ GHG fluxes to 100 m^2 plot

Site	Soil $CO_{2(eq)}$			Snag stem $CO_{2(eq)}$			Cumulative	
	mg CO_2 hr^{-1}	mg CH_4 hr^{-1}	mg N_2O hr^{-1}	mg CO_2 hr^{-1}	mg CH_4 hr^{-1}	mg N_2O hr^{-1}	Soil mg CO_2 hr^{-1}	Snag stem mg CO_2 hr^{-1}
PPP	34,569	4554	69	198	1.2	0.02	39,193	200
PC	22,385	4738	583	1158	53.6	− 1.1	27,706	1211
PP	29,593	9756	− 1477	416	89.9	− 0.4	37,873	506
GR	21,364	824	2443	441	53.2	79.3	24,631	573
SQ	32,507	1029	116	67	207.8	5.5	33,651	892

Soil GHG fluxes scaled up with live and dead tree basal area subtracted. Snag stem GHG fluxes scaled using DBH of snags measured and calculated cylindrical surface area up to 1.4 m. Median GHG fluxes for each site was used for scaling

account because ghost forests could collectively contribute a significant amount, as shown by the upscaling of these GHGs within a 100 m^2 plot (Table 6). This evidence also supports the need to estimate ghost forest GHG production, since there is no longer leaf canopy consuming CO_2 through photosynthesis, potentially making ghost forests major GHG sources.

Snag GHG fluxes in context

Our CO_2 flux rates from snags were slightly lower than other wetland regions, and 6–10 times lower than upland trees (Table 7). Snag CH_4 fluxes from our study were within the range of other wetland studies, except for Amazonian live tree species which were 1–2 orders of magnitude higher (Pangala et al. 2017). Live tree CH_4 fluxes in upland regions were generally much lower than wetlands. Our study also demonstrated the ability of some snags to uptake CH_4, which was also reported in a previous study within the same region (Carmichael et al. 2017). There is limited information on tree stem N_2O emissions (live and dead), but we were able to include N_2O fluxes from snags within the same area (unpublished) and are also within range as our study (Carmichael et al. 2017). Very few tree studies in wetland environments report N_2O fluxes, most likely due to the low magnitude and high variability of N_2O emissions. Live tree stem N_2O fluxes in uplands have been reported to be both sources and sinks, which is similar to what we found in our study for a few snags in Pocosin and Point Peter, although the majority of snags we measured were sources.

Conclusion

Although snag area over soils is small, snag GHGs collectively increased the total ecosystem $CO_{2(eq)}$ by 25%. Hydrological conditions and salinity significantly influenced soil GHG fluxes between the two field campaigns, but snags were less predictable. The environmental parameters that influence the production of CH_4 in soils however were often oppositely correlated with snag CH_4 fluxes. The disconnect between drivers in soil CH_4 and snag CH_4 production may have been due to oxidation of CH_4 within snag stem trunks, further highlighting the complexities of snags vs live trees. Our results also show that soil CH_4 fluxes contributed as much radiative forcing as CO_2 to the radiative balance during wet years. Although snag CH_4 and N_2O GHGs did not contribute as much as CO_2 they should still be taken into account given the cumulative amounts that they contribute. Salinity induced stress and increasing frequency of flooding events is projected for much of the coastal southeastern US (Sweet et al. 2018), which will lead to a decrease in primary productivity and an increase in the spatial extent of ghost forests (Krauss et al. 2009). This study demonstrates the potential snags have to emit GHGs to the atmosphere, but also how unpredictable they can be under various hydrological conditions and salinity levels. Therefore, more efforts should be done to include tree GHGs (both live and dead) in regional and global budgets.

Table 7 Comparison of median tree stem GHG fluxes from other studies (data table updated from Covey and Megonigal 2019)

Type	mg CO_2 m^{-2} h^{-1}	mg CH_4 m^{-2} h^{-1}	μg N_2O m^{-2} h^{-1}	Source	Citation
Wetlands	114.70	0.27	4.46	Dead	This Study (2018)
	118.68	0.33	3.49	Dead	This Study (2019)
	–	− 0.600	− 2.7	Dead	Carmichael et al. (2017)
	114.60	0.400	4.5	Dead	↑
	–	0.036	–	Live	Gauci et al. (2010)
	–	0.164	–	Dead	Jeffrey et al. (2019)
	-	0.020	–	Live	↑
	–	0.094	–	Live	Pangala et al. (2013)
	–	0.326	–	Live	Pangala et al. (2015)
	–	46.400	–	Live	Pangala et al. (2017)
	348.04	0.181	–	Live	Pitz et al. (2018)
	–	0.006	–	Live	Pulliam (1992)
	–	0.046	–	Live	Sjögersten et al. (2019)
	–	0.176	–	Live	Terazawa et al. (2007)
	–	0.693	–	Live	Terazawa et al. (2015)
Uplands	601.13	0.021	− 2.46	Live	Barba et al. (2019)
	–	0.187	–	Live	Covey et al. (2012)
	–	− 0.002	160.00	Live	Machacova et al. (2013)
	–	0.00005	0.03	Live	Machacova et al. (2016)
	69.74	–	0.11	Live	Machacova et al. (2019)
	295.00	-0.0015	− 3.0	Live	Machacova et al. (2021)
	182.16	0.015	–	Live	Maier et al. (2018)
	299.36	2.940	–	Live	Megonigal et al. (2020)
	–	0.0006	1.24	Live	Moldaschl et al. (2021)
	–	0.025	–	Live	Pitz and Megonigal (2017)
	–	0.0005	–	Live	Plain et al. (2019)
	–	0.094	–	Live	Wang et al. (2016)
	–	0.273	–	Live	Wang et al. (2017)
	670.03	-0.018	–	Dead	Warner et al. (2017)
	305.71	0.006	–	Live	↑
	–	0.094	636.50	Live	Welch et al. (2019)

Acknowledgements We thank Destinee Parson, Colin Dail, Cam Phipps, Margaret Maynardie, Kelsey Morton, and Steve Anderson for field and lab assistance. We are also thankful for the Ardón lab, Dr. Jodi Forrester, and Dr. Mary Jane Carmichael for feedback on this manuscript. This work was funded by National Science Foundation (DEB1713592) as well as North Carolina Sea Grant/SpaceGrant Fellowship (2019).

Author contributions All authors conceived the study and research methods. Material preparation, data collection and data analysis were performed by MM. The first draft of the manuscript was written by MM with feedback and comments from MA. All authors reviewed, edited, and approved the manuscript to its final form.

Funding This work was funded by National Science Foundation (DEB1713592) as well as North Carolina Sea Grant/SpaceGrant Fellowship (2019).

Data availability The datasets generated during and/or analyzed during the current study are available from the corresponding author at request.

Code availability The code used to process and analyzed data are available from the corresponding author at request.

Declarations

Conflict of interest The authors declare that the research was conducted in the absence of any commercial or financial relationships that could be construed as a potential conflict of interest.

References

Ardón M, Morse JL, Colman BP, Bernhardt ES (2013) Drought-induced saltwater incursion leads to increased wetland nitrogen export. Glob Change Biol 19:2976–2985. https://doi.org/10.1111/gcb.12287

Ardón M, Helton AM, Bernhardt ES (2018) Salinity effects on greenhouse gas emissions from wetland soils are contingent upon hydrologic setting: a microcosm experiment. Biogeochemistry 140:217–232. https://doi.org/10.1007/s10533-018-0486-2

Barba J, Poyatos R, Vargas R (2019) Automated measurements of greenhouse gases fluxes from tree stems and soils: magnitudes, patterns and drivers. Sci Rep Nat Publ Group Lond 9:1–13. https://doi.org/10.1038/s41598-019-39663-8

Carmichael MJ, Bernhardt ES, Bräuer SL, Smith WK (2014) The role of vegetation in methane flux to the atmosphere: should vegetation be included as a distinct category in the global methane budget? Biogeochemistry 119:1–24. https://doi.org/10.1007/s10533-014-9974-1

Carmichael MJ, Helton AM, White JC, Smith WK (2017) Standing dead trees are a conduit for the atmospheric flux of CH4 and CO2 from wetlands. Wetlands. https://doi.org/10.1007/s13157-017-0963-8

Chapin SF, Matson PA (2011) Principles of terrestrial ecosystem ecology. Springer, New York

Corbett DR, Vance D, Letrick E et al (2007) Decadal-scale sediment dynamics and environmental change in the albemarle estuarine system, North Carolina. Estuar Coast Shelf Sci 71:717–729. https://doi.org/10.1016/j.ecss.2006.09.024

Covey KR, Megonigal JP (2019) Methane production and emissions in trees and forests. New Phytol 222:35–51. https://doi.org/10.1111/nph.15624

Covey KR, Wood SA, Warren RJ et al (2012) Elevated methane concentrations in trees of an upland forest. Geophys Res Lett 39:L15705. https://doi.org/10.1029/2012GL052361

Gauci V, Gowing DJG, Hornibrook ERC et al (2010) Woody stem methane emission in mature wetland alder trees. Atmos Environ 44:2157–2160. https://doi.org/10.1016/j.atmosenv.2010.02.034

Helton A, Bernhardt E, Fedders A (2014) Biogeochemical regime shifts in coastal landscapes: the contrasting effects of saltwater incursion and agricultural pollution on greenhouse gas emissions from a freshwater wetland. Biogeochemistry 120:133–147. https://doi.org/10.1007/s10533-014-9986-x

Helton AM, Ardón M, Bernhardt ES (2019) Hydrologic context alters greenhouse gas feedbacks of coastal wetland salinization. Ecosystems 22:1108–1125. https://doi.org/10.1007/s10021-018-0325-2

Hornibrook ERC, Longstaffe FJ, Fyfe WS (1997) Spatial distribution of microbial methane production pathways in temperate zone wetland soils: Stable carbon and hydrogen isotope evidence. Geochim Cosmochim Acta 61:745–753. https://doi.org/10.1016/S0016-7037(96)00368-7

Huntington JL, Hegewisch KC, Daudert B et al (2017) Climate engine: cloud computing and visualization of climate and remote sensing data for advanced natural resource monitoring and process understanding. Bull Am Meteorol Soc 98:2397–2410. https://doi.org/10.1175/BAMS-D-15-00324.1

Hutchinson GL, Mosier AR (1981) Improved soil cover method for field measurement of nitrous oxide fluxes. Soil Sci Soc Am J 45:311–316. https://doi.org/10.2136/sssaj1981.03615995004500020017x

Jeffrey LC, Reithmaier G, Sippo JZ et al (2019) Are methane emissions from mangrove stems a cryptic carbon loss pathway? Insights from a catastrophic forest mortality. New Phytol 224:146–154. https://doi.org/10.1111/nph.15995

Jeffrey LC, Maher DT, Tait DR et al (2021) Isotopic evidence for axial tree stem methane oxidation within subtropical lowland forests. New Phytol. https://doi.org/10.1111/nph.17343

Kirwan ML, Gedan KB (2019) Sea-level driven land conversion and the formation of ghost forests. Nat Clim Change 9:450–457. https://doi.org/10.1038/s41558-019-0488-7

Kirwan ML, Megonigal JP (2013) Tidal wetland stability in the face of human impacts and sea-level rise. Nature 504:53–60. https://doi.org/10.1038/nature12856

Kohl L, Koskinen M, Rissanen K et al (2019) Technical note: interferences of volatile organic compounds (VOCs) on methane concentration measurements. Biogeosciences 16:3319–3332. https://doi.org/10.5194/bg-16-3319-2019

Kopp RE, Hay CC, Little CM, Mitrovica JX (2015) Geographic variability of sea-level change. Curr Clim Change Rep 1:192–204. https://doi.org/10.1007/s40641-015-0015-5

Krauss KW, Duberstein JA, Doyle TW et al (2009) Site condition, structure, and growth of baldcypress along tidal/non-tidal salinity gradients. Wetlands 29:505–519. https://doi.org/10.1672/08-77.1

Krauss KW, Noe GB, Duberstein JA et al (2018) The role of the upper tidal estuary in wetland blue carbon storage and flux. Glob Biogeochem Cycles. https://doi.org/10.1029/2018GB005897

Machacova K, Papen H, Kreuzwieser J, Rennenberg H (2013) Inundation strongly stimulates nitrous oxide emissions from stems of the upland tree fagus sylvatica and the riparian tree *Alnus glutinosa*. Plant Soil 364:287–301. https://doi.org/10.1007/s11104-012-1359-4

Machacova K, Bäck J, Vanhatalo A et al (2016) Pinus sylvestris as a missing source of nitrous oxide and methane in boreal forest. Sci Rep Nat Publ Group Lond. https://doi.org/10.1038/srep23410

Machacova K, Vainio E, Urban O, Pihlatie M (2019) Seasonal dynamics of stem N2O exchange follow the physiological

activity of boreal trees. Nat Commun. https://doi.org/10.1038/s41467-019-12976-y
Machacova K, Borak L, Agyei T et al (2021) Trees as net sinks for methane (CH4) and nitrous oxide (N2O) in the lowland tropical rain forest on volcanic Réunion Island. New Phytol 229:1983–1994. https://doi.org/10.1111/nph.17002
Maier M, Machacova K, Lang F et al (2018) Combining soil and tree-stem flux measurements and soil gas profiles to understand CH4 pathways in fagus sylvatica forests. J Plant Nutr Soil Sci 181:31–35. https://doi.org/10.1002/jpln.201600405
Manda AK, Giuliano AS, Allen TR (2014) Influence of artificial channels on the source and extent of saline water intrusion in the wind tide dominated wetlands of the southern Albemarle estuarine system (USA). Environ Earth Sci 71:4409–4419. https://doi.org/10.1007/s12665-013-2834-9
Megonigal JP, Brewer PE, Knee KL (2020) Radon as a natural tracer of gas transport through trees. New Phytol 225:1470–1475. https://doi.org/10.1111/nph.16292
Minick KJ, Mitra B, Li X et al (2019) Water table drawdown alters soil and microbial carbon pool size and isotope composition in coastal freshwater forested wetlands. Front For Glob Change. https://doi.org/10.3389/ffgc.2019.00007
Moldaschl E, Kitzler B, Machacova K et al (2021) Stem CH4 and N2O fluxes of fraxinus excelsior and populus alba trees along a flooding gradient. Plant Soil. https://doi.org/10.1007/s11104-020-04818-4
Moorhead KK, Brinson MM (1995) Response of wetlands to rising sea level in the lower coastal plain of North Carolina. Ecol Appl 5:261–271. https://doi.org/10.2307/1942068
Morse JL, Ardón M, Bernhardt ES (2012) Using environmental variables and soil processes to forecast denitrification potential and nitrous oxide fluxes in coastal plain wetlands across different land uses. J Geophys Res Biogeosci. https://doi.org/10.1029/2011JG001923
Neubauer SC (2013) Ecosystem responses of a tidal freshwater marsh experiencing saltwater intrusion and altered hydrology. Estuaries Coasts 36:491–507. https://doi.org/10.1007/s12237-011-9455-x
Neubauer SC, Megonigal JP (2015) Moving beyond global warming potentials to quantify the climatic role of ecosystems. Ecosystems 18:1000–1013. https://doi.org/10.1007/s10021-015-9879-4
Pangala SR, Moore S, Hornibrook ERC, Gauci V (2013) Trees are major conduits for methane egress from tropical forested wetlands. New Phytol 197:524–531. https://doi.org/10.1111/nph.12031
Pangala SR, J. GD, Hornibrook ERC, et al (2015) The contribution of trees to ecosystem methane emissions in a temperate forested wetland. Glob Change Biol 21:2642–2654. https://doi.org/10.1111/gcb.12891
Pangala SR, Enrich-Prast A, Basso LS et al (2017) Large emissions from floodplain trees close the Amazon methane budget. Nature 552:230–234. https://doi.org/10.1038/nature24639
Pedersen AR, Petersen SO, Schelde K (2010) A comprehensive approach to soil-atmosphere trace-gas flux estimation with static chambers. Eur J Soil Sci 61:888–902. https://doi.org/10.1111/j.1365-2389.2010.01291.x
Pitz S, Megonigal PJ (2017) Temperate forest methane sink diminished by tree emissions. New Phytol 214:1432–1439. https://doi.org/10.1111/nph.14559
Pitz SL, Megonigal JP, Chang C-H, Szlavecz K (2018) Methane fluxes from tree stems and soils along a habitat gradient. Biogeochemistry 137:307–320. https://doi.org/10.1007/s10533-017-0400-3
Plain C, Ndiaye F-K, Bonnaud P et al (2019) Impact of vegetation on the methane budget of a temperate forest. New Phytol 221:1447–1456. https://doi.org/10.1111/nph.15452
Poffenbarger HJ, Needelman BA, Megonigal JP (2011) Salinity influence on methane emissions from tidal marshes. Wetlands 31:831–842. https://doi.org/10.1007/s13157-011-0197-0
Pohlert T (2014) The pairwise multiple comparison of mean ranks Package (PMCMR). R Package 27(2019):9
Poulter B, Christensen NL, Halpin PN (2006) Carbon emissions from a temperate peat fire and its relevance to interannual variability of trace atmospheric greenhouse gases. J Geophys Res Atmos. https://doi.org/10.1029/2005JD006455
Prendergast-Miller MT, Baggs EM, Johnson D (2011) Nitrous oxide production by the ectomycorrhizal fungi paxillus involutus and tylospora fibrillosa. FEMS Microbiol Lett 316:31–35. https://doi.org/10.1111/j.1574-6968.2010.02187.x
Pulliam WM (1992) Methane emissions from cypress knees in a southeastern floodplain swamp. Oecologia 91:126–128. https://doi.org/10.1007/BF00317250
R Core Team (2020) R: a language and environment for statistical computing. Version 3.5.1. Vienna, Austria. http://www.R-project.org/
Reddy KR, DeLaune RD (2008) Biogeochemistry of wetlands science and applications. CRC Press, Boca Raton
Riggs SR, Cleary WJ, Snyder SW (1995) Influence of inherited geologic framework on barrier shoreface morphology and dynamics. Mar Geol 126:213–234. https://doi.org/10.1016/0025-3227(95)00079-E
Siegenthaler A, Welch B, Pangala SR et al (2016) Semi-rigid chambers for methane gas flux measurements on tree stems. Biogeosciences 13:1197–1207
Sjögersten S, Siegenthaler A, Lopez OR et al (2019) Methane emissions from tree stems in neotropical peatlands. New Phytol. https://doi.org/10.1111/nph.16178
Smart LS, Taillie PJ, Poulter B et al (2020) Aboveground carbon loss associated with the spread of ghost forests as sea levels rise. Environ Res Lett 15:104028. https://doi.org/10.1088/1748-9326/aba136
Sweet WV, Dusek G, Obeysekera J, Marra JJ (2018) Patterns and projections of high tide flooding along the U.S. coastline using a common impact threshold. NOAA, Washington, DC
Taillie PJ, Moorman CE, Poulter B et al (2019) Decadal-scale vegetation change driven by salinity at leading edge of rising sea level. Ecosystems 22:1918–1930. https://doi.org/10.1007/s10021-019-00382-w
Terazawa K, Ishizuka S, Sakata T et al (2007) Methane emissions from stems of *Fraxinus mandshurica* var. japonica trees in a floodplain forest. Soil Biol Biochem 39:2689–2692. https://doi.org/10.1016/j.soilbio.2007.05.013

Terazawa K, Yamada K, Ohno Y et al (2015) Spatial and temporal variability in methane emissions from tree stems of *Fraxinus mandshurica* in a cool-temperate floodplain forest. Biogeochem 123:349–362. https://doi.org/10.1007/s10533-015-0070-y

Ury EA, Yang X, Wright JP, Bernhardt ES (2021) Rapid deforestation of a coastal landscape driven by sea level rise and extreme events. Ecol Appl n/a:e2339. https://doi.org/10.1002/eap.2339

Wang Z-P, Gu Q, Deng F-D et al (2016) Methane emissions from the trunks of living trees on upland soils. New Phytol 211:429–439. https://doi.org/10.1111/nph.13909

Wang Z-P, Han S-J, Li H-L et al (2017) Methane production explained largely by water content in the heartwood of living trees in upland forests. J Geophys Res Biogeosci 122:2479–2489. https://doi.org/10.1002/2017JG003991

Warner DL, Villarreal S, McWilliams K et al (2017) Carbon dioxide and methane fluxes from tree stems, coarse woody debris, and soils in an upland temperate forest. Ecosystems 20:1205–1216. https://doi.org/10.1007/s10021-016-0106-8

Welch B, Gauci V, Sayer EJ (2019) Tree stem bases are sources of CH4 and N2O in a tropical forest on upland soil during the dry to wet season transition. Glob Change Biol 25:361–372. https://doi.org/10.1111/gcb.14498

Weston NB, Vile MA, Neubauer SC, Velinsky DJ (2011) Accelerated microbial organic matter mineralization following salt-water intrusion into tidal freshwater marsh soils. Biogeochemistry 102:135–151. https://doi.org/10.1007/s10533-010-9427-4

Wilson BJ, Servais S, Charles SP et al (2018) Declines in plant productivity drive carbon loss from brackish coastal wetland mesocosms exposed to saltwater intrusion. Estuaries Coasts. https://doi.org/10.1007/s12237-018-0438-z

Winton RS, Richardson CJ (2016) A cost-effective method for reducing soil disturbance-induced errors in static chamber measurement of wetland methane emissions. Wetl Ecol Manag 24:419–425. https://doi.org/10.1007/s11273-015-9468-5

Winton RS, Richardson CJ (2017) Top-down control of methane emission and nitrogen cycling by waterfowl. Ecology 98:265–277. https://doi.org/10.1002/ecy.1640

Winton RS, Moorman M, Richardson CJ (2016) Waterfowl impoundments as sources of nitrogen pollution. Water Air Soil Pollut 227:390. https://doi.org/10.1007/s11270-016-3082-x

Wobbrock JO, Findlater L, Gergle D, Higgins JJ (2011) The aligned rank transform for nonparametric factorial analyses using only anova procedures. In: Proceedings of the 2011 Annual Conference on Human Factors in Computing Systems—CHI '11. ACM Press, Vancouver, BC, Canada, p 143

Zhang L, Shao H, Wang B et al (2019) Effects of nitrogen and phosphorus on the production of carbon dioxide and nitrous oxide in salt-affected soils under different vegetation communities. Atmos Environ 204:78–88. https://doi.org/10.1016/j.atmosenv.2019.02.024